Renewable Energy 85 (2016) 598–609

Contents lists available at ScienceDirect

Renewable Energy

journal homepage: www.elsevier.com/locate/renene

Voltage stability constrained multi-objective optimal reactive power dispatch under load and wind power uncertainties: A stochastic approach

Seyed Masoud Mohseni-Bonab [a], Abbas Rabiee [a, *], Behnam Mohammadi-Ivatloo [b]

[a] Departemant of Electrical Engineering, University of Zanjan, Zanjan, Iran
[b] Faculty of Electrical and Computer Engineering, University of Tabriz, Tabriz, Iran

ARTICLE INFO

Article history:
Received 2 April 2015
Received in revised form
15 June 2015
Accepted 7 July 2015
Available online 16 July 2015

Keywords:
Active power losses
Multi-objective optimal reactive power dispatch (MO-ORPD)
Scenario-based uncertainty modeling
Stochastic programming
Voltage stability
Wind farms (WFs)

ABSTRACT

Optimal reactive power dispatch (ORPD) problem is an important problem in the operation of power systems. It is a nonlinear and mixed integer programming problem, which determines optimal values for control parameters of reactive power producers to optimize specific objective functions while satisfying several technical constraints. In this paper, stochastic multi-objective ORPD (SMO-ORPD) problem is studied in a wind integrated power system considering the loads and wind power generation uncertainties. The proposed multi objective optimization problem is solved using ε-constraint method, and fuzzy satisfying approach is employed to select the best compromise solution. Two different objective functions are considered as follow: 1) minimization of the active power losses and 2) minimization of the voltage stability index (named L-index). In this paper VAR compensation devices are modeled as discrete variables. Moreover, to evaluate the performance of the proposed method for solution of multi-objective problem, the obtained results for deterministic case (DMO-ORPD), are compared with the available methods in literature. The proposed method is examined on the IEEE-57 bus system. The proposed models are implemented in GAMS environment. The numerical results substantiate the capability of the proposed SMO-ORPD problem to deal with uncertainties and to determine the best settings of control variables.

1. Introduction

From the viewpoint of operation cost, environmental concerns and system security, optimal reactive power dispatch (ORPD) is important for power utilities operators. The ORPD is a specific subcategory of OPF problem, which optimizes objective functions such as transmission losses or voltage stability enhancement by adjusting the generators voltages set-points, allocating reactive power compensation in weak buses, adjusting transformers tap ratios, etc.

1.1. Literature review

ORPD can be divided into two categories considering the number of target objective functions. These two categories are single objective function (mostly minimizing power losses) or multi objective (with considering two or three objectives) ORPD.

In the single objective ORPD, intelligent search based optimization algorithms like seeker optimization algorithm (SOA) [1], harmony search algorithm [2], differential evolutionary-based method [3,4], and gravitational search algorithm (GSA) [5] have been developed to deal with the ORPD problem. In this category voltage stability enhancement index or system real power loss are minimizing separately. In Refs. [6], a method for coordinated optimal allocation of reactive power sources in AC–DC power systems using unified power flow controller (UPFC) is presented for minimization of the sum of the squares of the voltage deviations of all load buses. Management and scheduling of VAR generation to enhance the voltage stability margin (VSM) in the framework of optimal reactive power dispatch (ORPD) problem is proposed in Ref. [7]. A reformed particle swarm optimization (PSO) strategy for the ORPD in the presence of wind farms has been proposed in Refs. [8], where PSO merged with a feasible solution search (FSSPSO). Optimal active–reactive power dispatch (OARPD)

* Corresponding author.
E-mail addresses: s.m.mohsenibonab@ieee.org (S.M. Mohseni-Bonab), rabiee@znu.ac.ir (A. Rabiee), mohammadi@ieee.org (B. Mohammadi-Ivatloo).

http://dx.doi.org/10.1016/j.renene.2015.07.021

Nomenclature

Sets

N_B	set of buses
N_L	set of branches
N_G	set of generating units
N_W	set of wind farms
N_s	set of all possible scenarios
N_T	set of tap changing transformers
N_C	set of VAR compensators
N_{PQ}	set of system PQ buses
N_{PV}	set of system PV buses

Indices

k	index of objective functions
m	index of tap changing transformers
i/j	index of bus numbers
S	index of scenario numbers
ℓ	index of transmission lines
sl	index of slack bus

Parameters

π_s	probability of scenario s
π_d	probability of demand scenario d
π_w	probability of wind power generation scenario w
$Y_{ij}\angle\gamma_{ij}$	magnitude/angle of ij-*th* element of Y_{BUS} matrix (pu/radian)
$P_{G_i,s}$	active power production of generator at bus i in scenario s
$P_{G_i}^{min}/P_{G_i}^{max}$	minimum/maximum value for active power
$Q_{C_i}^{min}/Q_{C_i}^{max}$	minimum/maximum value for reactive power compensation at bus i in scenario s
T_m^{min}/T_m^{max}	minimum/maximum value for m-th tap changer settings
$P_{D_d}^{min}/P_{D_d}^{max}$	minimum/maximum value of real power demand at d-th load scenario
$P_{D_i,s}$	expected real power of the i-th bus in scenario s
$Q_{D_i,s}$	expected reactive power of the i-th bus in scenario s
$Q_{G_i}^{min}/Q_{G_i}^{max}$	minimum/maximum value for reactive power of generator at bus i
V_i^{min}/V_i^{max}	minimum/maximum value for voltage magnitude of the i-th bus
S_ℓ^{max}	maximum transfer capacity of line ℓ
v	wind speed in m/s
v_{in}^c/v_{out}^c	cut-in/out speed of wind turbine in m/s
v_{rated}	rated speed of wind turbine in m/s
P_W^{avl}	available wind power generation
$Q_{C_i}^b$	VAR compensation capacity in each step at bus i
$I_{C_i}^{min}/I_{C_i}^{max}$	minimum/maximum Reactive power compensation step at bus i
$cos(\varphi_{lag,i})/cos(\varphi_{lead,i})$	lag/lead power factor limits of the wind farms located at node i
$\zeta_{W_{i,s}}$	percentage of wind power rated capacity realized at scenario sin bus i
$P_{W_i}^r$	wind farm rated capacity installed in bus i

Variables

$\bar{x}_s$	vector of dependent variables in scenario s
$\bar{u}_s$	vector of control variables in scenario s
T_m	value of m-th tap changer setting (which connects buses i and j)
$V_{i,s}$	voltage magnitude of bus i in scenario s
$\theta_{i,s}$	voltage angle at bus i in scenario s
$S_{\ell,s}$	power flow of ℓ-th branch in scenario s
$P_{G_{sl},s}$	active power production of slack bus in scenario s
$P_{W_i,s}/Q_{W_i,s}$	active/reactive power produced by wind farm at scenario s
$Q_{W_i}^{min}/Q_{W_i}^{max}$	minimum/maximum value of reactive power produced by wind farm
$Q_{G_i,s}$	reactive power production of generator at bus i in scenario s
$I_{C_i,s}$	reactive power compensation step at bus i in scenario s
$Q_{C_i,s}$	reactive power compensation at bus i in scenario s
ϕ_k	individual value of k-*th* conflicting objective function
$\hat{\phi}_k$	normalized value of k-*th* objective function

Functions

PL_s	active power losses in scenario s
EPL	expected active power losses
EPL^L/EPL^U	minimum/maximum value for expected real power loss
$L_{max,s}$	L_{max} value in scenario s
EL_{max}	expected value of voltage stability enhancement index (L_{max})
EL_{max}^L/EL_{max}^U	minimum/maximum value of EL_{max}

problem resolved one-by-one with evolutionary calculation methods like as evolutionary programming (EP), PSO, differential evolution (DE) and hybrid differential evolution (HDE) in Ref. [9]. An enhanced load flow Jaccobian is presented in Ref. [10] to redispatch the reactive power. The proposed approximation used tangent vector approach to decrease operational loss in a vital area considering the voltage collapse possibility. In Ref. [11] a new objective function is proposed for the ORPD problem based on a local voltage stability index called DSY, which has a strong correlation with VSM. Hybridized multiple heuristic algorithms are widely used for solution of ORPD problem. For example, hybrid shuffled frog leaping algorithm (SFLA) and regional seek algorithm known as Nelder–Mead (NM-SFLA) [12], hybrid modified teaching–learning algorithm (MTLA) and double differential evolution (DDE) [13], hybrid modified imperialist competitive algorithm (MICA) and invasive weed optimization (IWO) [14], firefly algorithm (FA) and Nelder Mead (NM) simplex method [15] are used for ORPD solution. The most significant advantage of hybrid algorithms is higher speed of convergence to the optimal solution. A penalty function based method presented in Ref. [16] to convert discrete ORPD model to the continuous and differentiable one. In a recent study [17], to consider uncertainties in ORPD problem, the researchers used chance constrained programming to solve ORPD problem for minimizing active power losses. Nodal power injections and random branch outages are considered as uncertainty sources in this paper.

Voltage stability control is one of present-day challenges in power systems operation and control. In Ref. [18] a multi-period ORPD model is proposed which uses the concept of model predictive voltage control. In Ref. [19], the settings of reactive power compensation devices are determine based on new improved voltage stability index (IVSI) by using hybrid differential evolution (HDE) algorithm. Voltage stability constrained optimal power flow (VSC-OPF) problem with considering L_{Max} index is proposed by

Ref. [20] in a wind-integrated system. Also, improved genetic algorithm (IGA) is utilized in Ref. [20] for minimization L_{Max} and system total fuel cost. Also, a new index is introduce in Ref. [21] named reactive power loadability (Qloadability), which is used to determine the best location for the DSTATCOM to enhance voltage stability, in distribution networks. DFIG-based variable speed wind turbines are utilized.

The multi-objective ORPD (i.e. the second category), has attracted attention of researchers, recently. In this category, L_{Max} is considered with different objectives (usually real power loss). Non-dominated sorting genetic algorithm-II (NSGA-II) [22] and modified NSGA-II (MNSGA-II) [23] are applied to settle multi objective optimal reactive power dispatch (MO-ORPD). To justify the Pareto-front obtained using MNSGA-II, Pareto-front is created using several runs of single objective optimization with the weighted sum of objectives. Multi objective evolutionary algorithms (MOEAs) have been used in recent years to solve MO-ORPD. In these algorithms, active power losses, voltage stability enhancement and voltage deviation are optimized simultaneously by determination of optimal values of control variables. A modern hybrid fuzzy multi-objective evolutionary algorithm (HFMOEA) [24], advanced teaching learning based optimization (TLBO) algorithm [25], novel strength Pareto multi group search optimizer (SPMGSO) [26], chaotic upgraded PSO based multi-objective optimization (MOCIPSO) and greatly enhanced PSO-based multi-objective optimization (MOIPSO) approaches [27] and chaotic parallel vector evaluated interactive honey bee mating optimization (CPVEIHBMO) [28] are examples of the recently presented algorithms for solution of MO-ORPD.

The existing wind farms are usually employing variable speed turbine technology. In this context, doubly fed induction generators (DFIGs) and permanent magnet synchronous generators (PMSG) are attractive choices. These machines are able to exchange reactive power with the AC network they connected. In Ref. [29], a detailed model of capability curve for DFIG is developed. This model is utilized in Refs. [30] and [31] to incorporate wind farms in the OPF problem. Also, PMSG is basically synchronous generators and the corresponding capability curve is well known.

1.2. Contributions

This paper is mainly focused on solving the MO-ORPD problem in a wind integrated power system considering the associated uncertainties. Demand and wind power generations are considered as sources of uncertainties in this work. The normal probability distribution function (PDF) and Rayleigh (PDF) are used for modeling the load and wind speed uncertainties, respectively. Two objective functions, namely active power losses minimization and voltage stability index (L_{max}) minimization are considered. The multi-objective problem is handled using ε-constraint technique and optimal Pareto set is attained. In this paper, for the sake of comparison with available methods, the reactive power compensation by shunt VAR compensators is modeled as continuous variable in deterministic MO-ORPD (i.e DMO-ORPD), while because of demonstrating real world problem, discrete model is adopted for these compensating devices in the proposed stochastic MO-ORPD (SMO-ORPD). The DMO-ORPD is NLP and the SMO-ORPD is MINLP optimization problem, which both are implemented in GAMS [32], and solved by SNOPT [33] and SBB [34] solvers.

Given the above descriptions, the highlights of this paper are as follows:

1) Modeling and including stochastic nature of loads and wind generations in the MO-ORPD problem (i.e. SMO-ORPD problem).
2) Discrete steps for shunt VAR compensation devices are used in the proposed SMO-ORPD problem. Most of the pervious literature used continuous modeling for capacitor banks.
3) To make use of ε-constraint technique and fuzzy satisfying method for solving and choosing the best compromise solution of MO-ORPD problem.

1.3. Paper organization

The remainder of this paper is set out as follows: Section 2 provides scenario based uncertainty modeling of stochastic parameters. In Section 3, complete formulation of MO-OPRD problem is presented. Section 4 gives the numerical results. Finally, conclusions of this paper are summarized in Section 5.

2. Uncertainty modeling

2.1. Demand uncertainty characterization via scenario based modeling

Due to stochastic nature of the load demand in electric power systems, it is required to model the load uncertainty in operation and planning of power systems. Generally load uncertainty can be modeled using the normal of Gaussian PDF [35]. In this paper, it is assumed that the mean and standard deviation of the load PDF, i.e. μ_D and σ_D are known. Probability of d-th load scenario is shown by π_d and calculated using Fig. 1 as follows. It is worth to note that $P_{D_d}^{\min}$ and $P_{D_d}^{\max}$ are the boundaries of d-th interval (or d-th load scenario), as shown in Fig. 1.

$$\pi_d = \int_{P_{D_d}^{\min}}^{P_{D_d}^{\max}} \frac{1}{\sqrt{2\pi\sigma^2}} exp\left[-\frac{(P_D-\mu_D)^2}{2\sigma^2}\right] dP_D \tag{1}$$

$$P_{D_d} = \frac{1}{\pi_d} \times \int_{P_{D,d}^{\min}}^{P_{D,d}^{\max}} \left(P_D \times \frac{1}{\sqrt{2\pi\sigma^2}} exp\left[-\frac{(P_D-\mu_D)^2}{2\sigma^2}\right]\right) dP_D \tag{2}$$

2.2. Wind power generation uncertainty modeling

Generally the wind speed uncertainty is modeled using the Rayleigh or Weibul PDF [36]-[31]. It should be mentioned that the Weibull distribution is a generalized form of the Rayleigh PDF. The Rayleigh PDF of the wind speed can be expressed as follows:

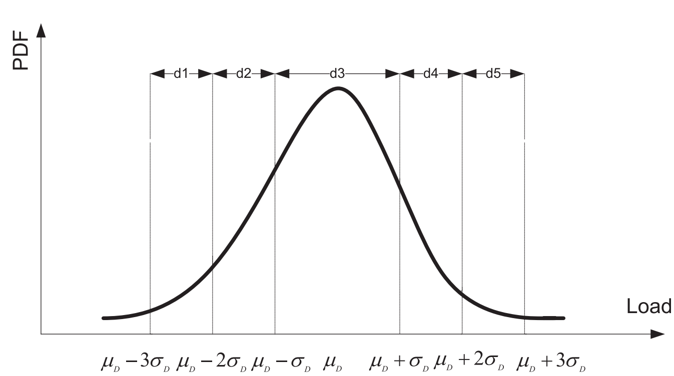

Fig. 1. The load PDF and load uncertainty scenarios generation.

$$PDF(v) = \left(\frac{v}{c^2}\right) exp\left[-\left(\frac{v}{\sqrt{2}c}\right)^2\right] \quad (3)$$

The wind speed variation range is divided into intervals, which is called scenarios. The probability of each scenario can be calculated from the following equation. The occurrence probability of scenario s and the corresponding wind speed v_s is calculated as follows:

$$\pi_W = \int_{v_{i,w}}^{v_{f,w}} \left(\frac{v}{c^2}\right) exp\left[-\left(\frac{v}{\sqrt{2}c}\right)^2\right] dv \quad (4)$$

$$v_W = \frac{1}{\pi_W} \times \int_{v_{i,w}}^{v_{f,w}} \left(v \times \left(\frac{v}{c^2}\right) exp\left[-\left(\frac{v}{\sqrt{2}c}\right)^2\right]\right) dv \quad (5)$$

where, v_W is the wind speed at w-th wind scenario, and $v_{i,w}$, $v_{f,w}$ are the starting and ending points of wind speed's interval at w-th scenario, respectively. Also, c is scaling parameter which is obtained by historical wind data.

The characteristic curve of a wind turbine determines the relation between the available wind speed and generated wind power. A linearized characteristics curve is presented in Fig. 2 [37]. Using this curve, the forecasted output power of the wind turbine for different wind speeds can be obtained using the following equation.

$$P_W^{avl} = \begin{cases} 0 & v_W \le v_{in}^c \text{ or } v_W \ge v_{out}^c \\ \dfrac{v_W - v_{in}^c}{v_{rated} - v_{in}^c} P_r^w & v_{in}^c \le v_W \le v_{rated} \\ P_r^w & v_{rated} \le v_W \le v_{out}^c \end{cases} \quad (6)$$

By generating the proper number of scenarios for wind power and load demand, the overall number of combined wind-load scenarios is obtained by multiplying the number of wind and load individual scenarios. The probability of scenario s, which is obtained considering w-th scenario of wind and d -th scenario of load demand, can be obtained using the following equation.

$$\pi_s = \pi_W \times \pi_d \quad (7)$$

2.3. Two stage stochastic optimization framework

In this paper two-stage stochastic programming method is used for decision making in an uncertain environment. In this method,

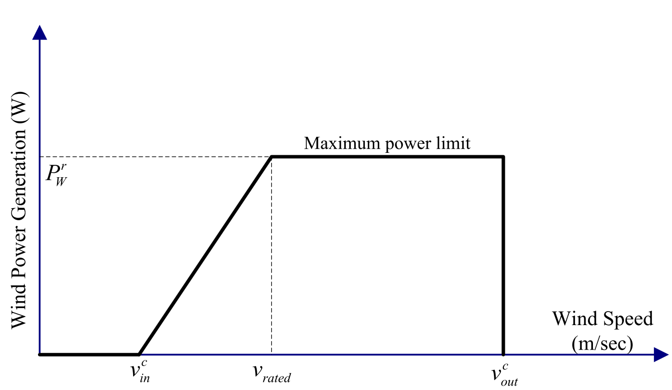

Fig. 2. The power curve of a wind turbine (rotor speed control regions).

the decision variables are categorized as "*here and now*" and "*wait and see*" variables [38]. The optimal values of "*here and now*" or "*first stage*" variables should be determined before realization of scenarios. In other words, their values are scenario independent and are same for all scenarios. In other hand, the optimal values of "*wait and see*" or "*second stage*" variables should be determined after realization of the scenarios. In other words, their values are scenario dependent and may be different for different scenarios. In the proposed SMO-ORPD problem the decision variables (DVs) are generator voltages, tap values of tap changing transformers and the amount of reactive power compensations in the weak buses.

3. Problem formulation

In this section, the studied objective functions, description of ε-constraint method for dealing with the SMO-ORPD, fuzzy satisfying method for selection of the best compromise solution of Pareto front and problem constraints like load flow equations are described.

3.1. Objective functions

Voltage stability of the power system is strongly correlated with reactive power management of the system. Hence, voltage stability improvement is also considered as another objective function besides the total power losses. These objective functions may be conflicted [39]-[27]. The ORPD problem variables subsets can be stated as follows.

$$\begin{aligned} \overline{u} &= \begin{bmatrix} V_i & ,\forall i \in N_G & \\ T_m & ,\forall m \in N_T & \\ Q_{C_i,s} & ,\forall i \in N_C & ,\forall s \\ P_{W_i,s} & ,\forall i \in N_W & ,\forall s \\ Q_{W_i,s} & ,\forall i \in N_W & ,\forall s \end{bmatrix} \\ \overline{x} &= \begin{bmatrix} V_{i,s} & ,\forall i \in N_{PQ} & ,\forall s \\ \theta_{i,s} & ,\forall i \in N_B & ,\forall s \\ S_{\ell,s} & ,\forall \ell \in N_L & ,\forall s \\ Q_{G_i,s} & ,\forall i \in N_G & ,\forall s \\ P_{G_i,s} & ,\forall i = sl & ,\forall s \end{bmatrix} \end{aligned} \quad (8)$$

where, $\overline{u}$ is the set of control variables, and $\overline{x}$ is the set of state variables. As it is aforementioned, the set of control variables is divided into two distinct subsets, i.e. *here and now* and *wait and see* control variables. The set of here and now decision variables (D_{HN}) are as follows:

$$D_{HN} = \begin{Bmatrix} V_i & ,\forall i \in N_G \\ T_m & ,\forall m \in N_T \end{Bmatrix} \quad (9)$$

Also, the set of wait and see decision variables (D_{WS}) are as follows.

$$D_{WS} = \begin{Bmatrix} Q_{C_i,s} & ,\forall i \in N_C & ,\forall s \\ P_{W_i,s} & ,\forall i \in N_W & ,\forall s \\ Q_{W_i,s} & ,\forall i \in N_W & ,\forall s \end{Bmatrix} \quad (10)$$

3.1.1. Minimization of total active power losses

Minimization the total power losses in transmission system is important objective in power systems for improvement of the total energy efficiency and economic reasons. The active power losses in scenario s can be mathematically expressed as follows.

$$PL_s(\overline{u}_s, \overline{x}_s) = \sum_{i=1}^{N_G} P_{G_i,s} + \sum_{i=1}^{N_W} P_{W_i,s} - \sum_{i=1}^{N_B} P_{D_i,s} \quad (11)$$

Expected value of power losses (EPL) over the whole scenarios is considered as the first objective function. It is calculated as follows.

$$\phi_1 = EPL = \sum_{s=1}^{N_s} \left(\pi_s \times PL_s(\overline{u}_s, \overline{x}_s)\right) \tag{12}$$

3.1.2. Minimization of voltage stability index (L-index)

Several methods can be used for incorporating static voltage stability enhancement in ORPD problem. For example, power–voltage curves is implemented in Ref. [40] for static voltage stability modeling. Minimum singular value of the load flow Jacobian matrix [41] and minimum L-index [42] are other indices used for determining the voltage stability margin of the system. In this paper L-index is chosen for quantifying voltage stability. This index shows the distance of the current state of power system from the voltage stability limit point, which is computed based on power flow solution. It should be mentioned that the value of L-index varies between 0 and 1. L-index value less than 1 (voltage collapse point) and close to 0 (no load point) corresponds with more voltage stability margin. The voltage magnitude and phase angle of network buses are functions of system load and generation. By increasing the transmitted power and for near maximum power transfer condition, the voltage stability index values for load buses becomes closer to 1, which indicates that the system is closer to voltage collapse. For any load node j, L-index can be expressed as [25]:

$$L_j = \left|1 - \sum_{i=1}^{N_G} F_{ji} \frac{\overline{V}_i}{\overline{V}_j}\right| = \sqrt{\left(1 - \sum_{i=1}^{N_G} \eta_{ji} cos(\vartheta_{ji})\right)^2 + \left(\sum_{i=1}^{N_G} \eta_{ji} \sin(\vartheta_{ji})\right)^2}, \quad \forall j \in N_{PQ} \tag{13}$$

where, $\overline{V}_i = V_i \angle \theta_i$ and $\overline{V}_j = V_j \angle \theta_j$. Also η_{ji} and ϑ_{ji} are calculated using the following equations.

$$\begin{cases} \eta_{ji} = |F_{ji}| \dfrac{V_i}{V_j} \\ \vartheta_{ji} = \alpha_{ji} + \theta_i - \theta_j \end{cases} \tag{14}$$

In order to calculate F_{ji}, the system Y_{BUS} matrix is rearranged as follows:

$$\begin{bmatrix} I_L \\ I_G \end{bmatrix} = \begin{bmatrix} Y_{GG} & Y_{GL} \\ Y_{LG} & Y_{LL} \end{bmatrix} \begin{bmatrix} V_L \\ V_G \end{bmatrix} \tag{15}$$

With this rearrangement, F_{ji} in (13) can be expressed as:

$$F = -[Y_{LL}]^{-1}[Y_{LG}] \tag{16}$$

Since F is a complex matrix, then it is represented by its polar form, i.e.

$$F = \left[|F_{ji}| \angle \alpha_{ji}\right], \quad (\forall j \in N_{PQ}, i \in N_G) \tag{17}$$

Thus, for each scenario s, the maximum value of L-index among all load buses is considered as the voltage stability index as follows:

$$L_{max_s}(\overline{u}_s, \overline{x}_s) = \max(L_j) \quad , j \in N_{PQ} \tag{18}$$

The second objective (i.e. ϕ_2) is the expected value of L_{max} for all scenarios, which is obtained from (18):

$$\phi_2 = EL_{\max} = \sum_{s=1}^{N_s} \left(\pi_s \times L_{max_s}(\overline{u}_s, \overline{x}_s)\right) \tag{19}$$

3.2. ε–constraint method

ε–constraint method [35] is an approach in which the multi-objective optimization problem is converted to a conventional single-objective problem. In this method, all objective functions except one, treated as inequality constraints by defining proper value of control parameter named as ε parameter. In the proposed SMO-ORPD problem, ϕ_1 is optimized while ϕ_2 is considered as a constraint as follows.

$$OF = \min(\phi_1) \tag{20}$$

$$s.t: \begin{cases} \phi_2 \le \varepsilon \\ (25) - (35) \end{cases} \tag{21}$$

It is observed from Fig. 3 and Equations (20) and (21) that ϕ_2 (i.e. EL_{max}) is constrained by the parameter ε. This parameter varies from the minimum value to the maximum value of ϕ_2 (i.e. from ϕ_2^L to ϕ_2^U) gradually, and for any value of ε, the modified single objective optimization problem (i.e. (20), (21)) is solved, and the optimal solutions like point C in Fig. 3 are obtained. It is noteworthy that in (21) the constraints of the original multi-objective optimization problem, i.e. (25)–(35), which are described in Section 3.4), are also included. The set of all obtained solutions for the entire variations of ε (from ϕ_2^L to ϕ_2^U) are Pareto optimal front of the multi-objective optimization problem.

3.3. Fuzzy decision maker

By solving the MO-ORPD problem a Pareto front is derived and it is required to select the best solution from this Pareto optimal set. Fuzzy decision maker is used in this paper for this purpose. In the method a fuzzy membership function is assigned to each solution in the Pareto front. The fuzzy membership is in the interval [0, 1]. The linear fuzzy membership functions can be obtained for the i-th objective function of $\widehat{\phi}_k$ using the following equation [35].

$$\widehat{\phi}_k = \begin{cases} 1 & \phi_k \le \phi_k^L \\ \dfrac{\phi_k - \phi_k^U}{\phi_k^L - \phi_k^U} & \phi_k^L \le \phi_k \le \phi_k^U \\ 0 & \phi_k \ge \phi_k^U \end{cases} \tag{22}$$

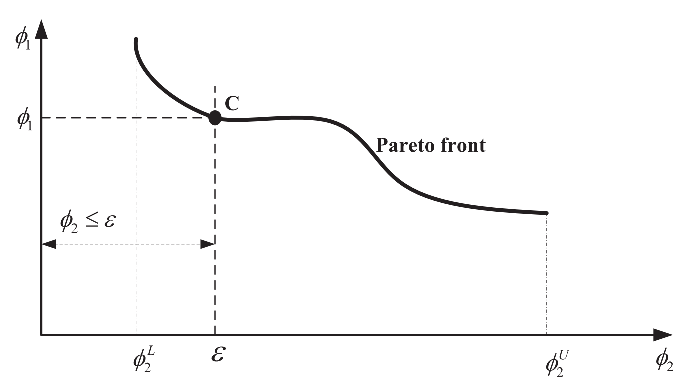

Fig. 3. Description of ε–constraint method.

The best compromise solution can be selected using the min–max method described in Ref. [43]. In the min–max method minimum value of $\widehat{\phi}_1$ and $\widehat{\phi}_2$ for each solution is determined, and the solution with maximum value of $\min(\widehat{\phi}_1, \widehat{\phi}_2)$ is selected as the best compromise solution. In this paper, $\widehat{\phi}_1$ and $\widehat{\phi}_2$ are calculated as follows.

$$\widehat{\phi}_1 = \frac{EPL - EPL^U}{EPL^L - EPL^U} \tag{23}$$

$$\widehat{\phi}_2 = \frac{EL_{max} - EL^U_{max}}{EL^L_{max} - EL^U_{max}} \tag{24}$$

3.4. Constraints

3.4.1. Equality constraints (AC power balance equations)

The obtained solution should satisfy the power flow equations, which are described mathematically in the following.

$$\begin{cases} P_{G_i,s} + P_{W_i,s} - P_{D_i,s} = V_{i,s}\sum_{j=1}^{N_B} V_{j,s}Y_{ij}\cos(\theta_{i,s} - \theta_{j,s} - \gamma_{ij}) \\ Q_{G_i,s} + Q_{W_i,s} + Q_{C_i,s} - Q_{D_i,s} = V_{i,s}\sum_{j=1}^{N_B} V_{j,s}Y_{ij}\sin(\theta_{i,s} - \theta_{j,s} - \gamma_{ij}) \end{cases} \tag{25}$$

3.4.2. Inequality constraints on control/dependent variables

The active power, reactive power generation of the generators and voltage of buses should be in the allowed range as follows:

$$P^{min}_{G_i} \le P_{G_{sl},s} \le P^{max}_{G_i} \quad , \forall i = sl, \quad \forall s \tag{26}$$

$$Q^{min}_{G_i} \le Q_{G_i,s} \le Q^{max}_{G_i} \quad , \forall i \in N_G, \quad \forall s \tag{27}$$

$$V^{min}_{i} \le V_{i,s} \le V^{max}_{i} \quad , \forall i \in N_B, \quad \forall s \tag{28}$$

The power transmitted from the branches is constrained to its maximum value as follows.

$$|S_{\ell,s}| \le S^{max}_{\ell}, \quad \forall \ell \in N_L, \quad \forall s \tag{29}$$

The tap amounts of tap changers are also limited as follows.

$$T^{min}_{m} \le T_m \le T^{max}_{m} \quad , \forall m \in N_T \tag{30}$$

It is worth to note that the reactive power output of VAR compensation devices are modeled as a multi-step compensation, i.e. a discrete variable is defined for each VAR compensation node as follows, which determine how many steps of VAR injections are necessary.

$$Q_{C_i,s} = Q^b_{C_i} \times I_{C_i,s} \quad , \forall i \in N_C, \quad \forall s \tag{31}$$

The reactive power compensation steps are limited as follows.

$$I^{min}_{C_i} \le I_{C_i,s} \le I^{max}_{C_i} \quad \forall i \in N_C \ , \quad \forall s \tag{32}$$

Also, for the available active/reactive power outputs of wind farms, the following constraints are considered:

$$0 \le P_{W_i,s} \le \zeta_{W_{i,s}} \times P^r_{W_i} \quad , \forall i \in N_W, \quad \forall s \tag{33}$$

$$Q^{min}_{W_i} \le Q_{W_i,s} \le Q^{max}_{W_i} \quad , \forall i \in N_W \ , \forall s \tag{34}$$

In this paper, the reactive power output of wind farms are limited to the corresponding active power output as follows.

$$\begin{cases} Q^{max}_{W_i} = tg(\varphi_{lag}) \times P_{W_i,s} \\ Q^{min}_{W_i} = -tg(\varphi_{lead}) \times P_{W_i,s} \end{cases} \tag{35}$$

This means that in those scenarios in which the active power output of wind farm decreases, the reactive power injection is also restricted accordingly.

4. Case study and numerical results

Simulations are performed on the IEEE 57-bus test system. In order to clearly illustrate the effectiveness of proposed method, different cases are studied as follows:

(A) Deterministic optimization without wind farms (by ignoring the uncertainties of load and wind farms).
(B) Stochastic optimization with wind farms and load uncertainties (uncertainty characterization using scenario based approach).

For sake of comparison with the existing literature, the VAR compensation devices are modeled as continuous control variables in case (A). While, in case (B) the VAR compensations are modeled with discrete steps as described in the previous section.

4.1. Description of IEEE 57-bus system

IEEE 57-bus system consists of 57 buses and 7 generator buses [44], as shown in Fig. 4. Bus 1 is the slack bus. The network consists of 80 branches in which 14 branches are under load tap changing transformers. The reactive power compensation buses are buses 18, 25 and 53 [39], and each step of VAR compensation is assumed to be 0.5 MVAR. The load flow data and initial operating condition of the system are given in Ref. [45].

4.2. Scenario generation

Scenario generation technique was described in Section 2. In this paper, normal PDF is considered for uncertainty modeling of loads active and reactive power demand. The mean value of this PDF is the rated power of loads given in Ref. [45]. The standard deviation is assumed to be 2% of the mean load. Also, the entire PDF of loads is divided into five distinct areas and hence five scenarios are considered for loads. The amounts of average load in all scenarios along with their corresponding probabilities are given in Table 1.

Also, it assumed that a 250 MW wind farm is located at bus 52. The parameters of wind speed PDF and the corresponding wind power generation scenarios for this wind farm are adopted from Ref. [46]. There are five wind power generation scenarios, which their characteristics are summarized in Table 1. Finally, the total 25 wind-load scenarios along with the corresponding probabilities are given in Table 1.

4.3. Case-A: DMO-ORPD without WF

In this case, the Pareto front is obtained for IEEE 57-bus test system without considering any uncertainty and without wind power integration. The VAR compensation devices are modeled by continuous variables for the sake of comparison with the previous literature. The data of compensation limits are available in Appendix (Table A1). Table 2 summarizes the obtained Pareto

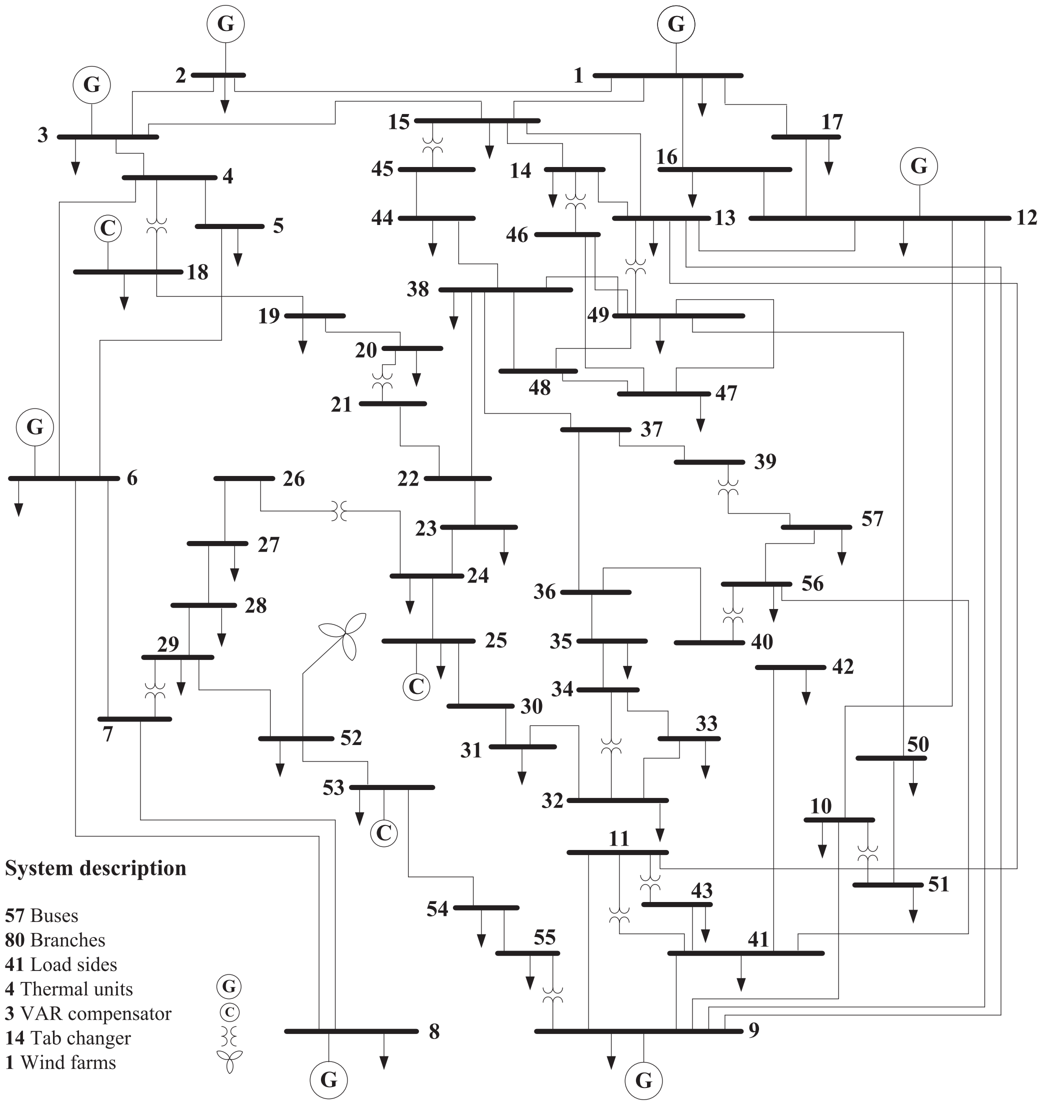

Fig. 4. Single line diagram of IEEE 57-bus test system.

solutions for this case. By using min–max fuzzy satisfying method, it is evident from Table 2 that the best compromise solution is *Solution#4*, with the maximum weakest membership function of 0.8303. The corresponding *PL* and L_{max} are equal to 25.0137 MW and 0.2290, respectively. For this solution, the optimal values of control variables are given in Table 3. It is also noteworthy that *Solution#1* corresponds to the loss minimization case, i.e. in *Solution#*, only *PL* is minimized, and the minimum value of *PL* is obtained 22.9486 MW. The Pareto optimal front of the two objective functions in case-A is depicted in Fig. 5.

Also, the obtained active power losses is compared with the results reported by some recently published algorithms. Fig. 6 shows the obtained results for *Solution#1* where the aim is to minimize the active power losses individually. According to this figure, it can be evidently observed that the obtained solution is superior to the previously reported ones like as seeker optimization algorithm (SOA) [39], comprehensive learning particle swarm optimizer (CLPSO) [39], local differential evolution (L-DE) [39], harmony search algorithm (HSA) [2], simple genetic algorithm (SGA) [2], conventional PSO (C–PSO) [12] and gravitational search algorithm (GSA) [5]. It is worth to mention that, since the above references reported the results for only minimization of active power losses, thus the results obtained in *Solution#1* are compared with their reported ones.

4.4. Case-B: SMO-ORPD with WF

In this case the load and wind power uncertainties are considered in the MO-ORPD using the previously described two stage stochastic programming approach. The attained Pareto optimal solutions in this case are presented in Table 4. It is inferred from this table that the *EPL* varies from 21.5119 MW to 26.1406 MW, whereas the EL_{max} varies from 0.255 to 0.2069, respectively. The *Solution#1* corresponds to the *EPL* minimization case, where the minimum value of 21.5119 MW is obtained for *EPL*, whereas *Solution#20* deals with the case of EL_{max} minimization, in which the minimum value of EL_{max} is 0.2069. It is observed from Table 5 that *Solution#5* is the best compromise solution, with *EPL* equals to 22.4864 MW and EL_{max} equals to 0.2188. Also, Fig. 7 depicts the obtained optimal Pareto front in this case.

Table 5 summarizes the obtained optimal *here and now* control variables for the best compromise solution. Also, the optimal values

Table 1
Wind/load scenarios with the corresponding individual and mixed probabilities.

			Scenario number	Load (%)	Wind (%)	π_s
load scenarios			s_1	95	0	0.0017
			s_2	95	12.87	0.0051
	Load (%)	π_d	s_3	95	49.37	0.0101
d_1	95	0.025	s_4	95	86.83	0.005
d_2	97	0.135	s_5	95	100	0.0031
d_3	100	0.680	s_6	97	0	0.0093
d_4	103	0.135	s_7	97	12.87	0.0276
d_5	105	0.025	s_8	97	49.37	0.0546
			s_9	97	86.83	0.0269
			s_{10}	97	100	0.0166
			s_{11}	100	0	0.0469
			s_{12}	100	12.87	0.139
			s_{13}	100	49.37	0.2753
			s_{14}	100	86.83	0.1355
Wind power generation scenarios			s_{15}	100	100	0.0834
			s_{16}	103	0	0.0093
			s_{17}	103	12.87	0.0276
	Wind (%)	π_w	s_{18}	103	49.37	0.0546
w_1	0	0.0689	s_{19}	103	86.83	0.0269
w_2	12.87	0.2044	s_{20}	103	100	0.0166
w_3	49.37	0.4048	s_{21}	105	0	0.0017
w_4	86.83	0.1992	s_{22}	105	12.87	0.0051
w_5	100	0.1227	s_{23}	105	49.37	0.0101
			s_{24}	105	86.83	0.005
			s_{25}	105	100	0.0031

Table 2
Pareto optimal solutions for DMO-ORPD without WFs (Case-A). The bold values correspond to the Pareto optimal solution.

#	*PL (MW)*	L_{max}	$\hat{\phi}_1$	$\hat{\phi}_2$	$\min(\hat{\phi}_1, \hat{\phi}_2)$
1	22.9486	0.2644	1.0000	0.0000	0.0000
2	23.6370	0.2347	0.9474	0.6962	0.6962
3	24.3253	0.2312	0.8947	0.7789	0.7789
4	**25.0137**	**0.2290**	**0.8421**	**0.8303**	**0.8303**
5	25.702	0.2275	0.7895	0.8657	0.7895
6	26.3904	0.2264	0.7368	0.8925	0.7368
7	27.0787	0.2255	0.6842	0.9139	0.6842
8	27.7671	0.2247	0.6316	0.9316	0.6316
9	28.4554	0.2241	0.5789	0.9466	0.5789
10	29.1438	0.2235	0.5263	0.9595	0.5263
11	29.8321	0.2230	0.4737	0.9706	0.4737
12	30.5205	0.2227	0.4210	0.9795	0.4210
13	31.2088	0.2224	0.3684	0.9861	0.3684
14	31.8972	0.2222	0.3158	0.9904	0.3158
15	32.5855	0.2221	0.2632	0.9935	0.2632
16	33.2739	0.2220	0.2105	0.9959	0.2105
17	33.9622	0.2219	0.1579	0.9977	0.1579
18	34.6506	0.2218	0.1053	0.9989	0.1053
19	35.3389	0.2218	0.0526	0.9996	0.0526
20	36.0273	0.2218	0.0000	1.0000	0.0000

of *wait and see* control variables are depicted in Figs. 8–10, in all possible scenarios. Fig. 8 shows the active power generation at the slack bus (i.e. bus 1) in all 25 scenarios. Besides, Fig. 9 depicts the active/reactive power output of the wind farm in all scenarios. The optimal amount of reactive power compensation steps in the buses 18, 25 and 53 are also given in Fig. 10.

5. Conclusions

The stochastic multi-objective optimal reactive power dispatch (SMO-ORPD) problem in a wind integrated power system is studied in this paper taking into account the uncertainties of system load and wind power generations. A two-stage stochastic optimization model is implemented for decision making under the above uncertainties. Real power losses and voltage stability enhancements

Table 3
Optimal control variables for the best compromise solution (i.e. *Solution#4*) in Case-A.

Control variable	#	DMO-ORPD (Case-A)
Generator Control variable	V_{G1} (pu)	1.013
	V_{G2} (pu)	1.0005
	V_{G3} (pu)	0.9868
	V_{G6} (pu)	0.9908
	V_{G8} (pu)	0.9941
	V_{G9} (pu)	0.9795
	V_{G12} (pu)	0.9655
	P_{G1} (MW)	445.8137
Transformer Tap changer (pu)	T_1	1.0009
	T_2	0.9844
	T_3	1.0022
	T_4	0.9856
	T_5	0.9519
	T_6	0.9926
	T_7	0.9836
	T_8	1.0076
	T_9	0.9946
	T_{10}	0.9668
	T_{11}	0.9000
	T_{12}	1.0217
	T_{13}	1.0320
	T_{14}	1.0025
VAR Compensation (MVAR)	Q_{C18}	10.0000
	Q_{C25}	5.9109
	Q_{C53}	6.3418

index (L-index) are optimized simultaneously in a multi objective optimization framework. The ε-constraint method is used to solve multi-objective optimization problem. To verify the effectiveness and optimality of the proposed model, the obtained results in the deterministic case are compared with the recently applied intelligent search-based algorithms and it is found that the proposed method can find better solutions for both objective functions in this case.

In the stochastic case, a comprehensive set of decision variables including *here and now* and *wait and see* control variables

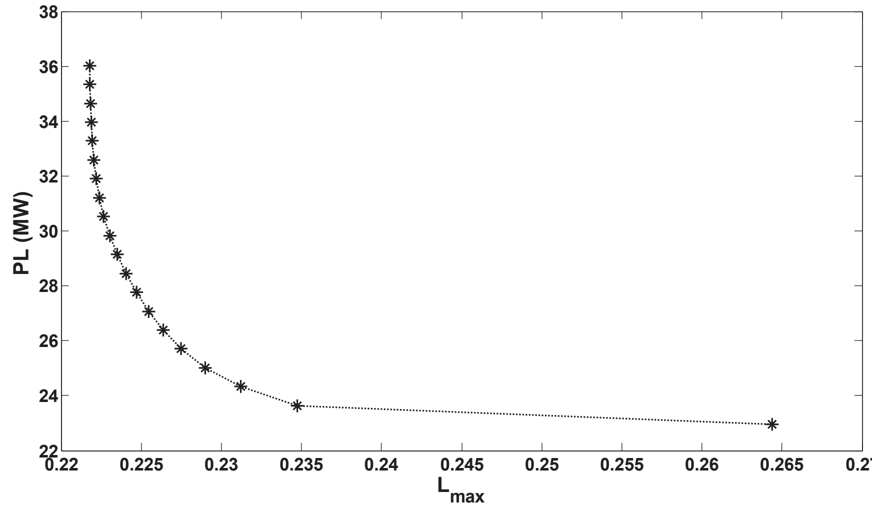

Fig. 5. Pareto optimal front for DMO-ORPD problem (Case-A).

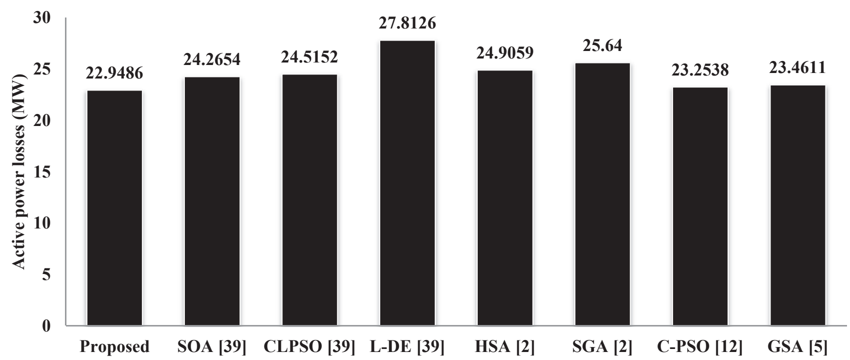

Fig. 6. Comparison of the obtained active power losses with the reported values in the literature (Case-A).

Table 4
Pareto optimal solutions for SMO-ORPD (Case-B). The bold values correspond to the Pareto optimal solution.

#	*EPL (MW)*	EL_{max}	$\hat{\phi}_1$	$\hat{\phi}_2$	$\min(\hat{\phi}_1, \hat{\phi}_2)$
1	21.5119	0.2550	1.0000	0.0000	0.0000
2	21.7555	0.2273	0.9474	0.5747	0.5747
3	21.9991	0.2236	0.8947	0.6532	0.6532
4	22.2427	0.2209	0.8421	0.7078	0.7078
5	**22.4864**	**0.2188**	**0.7895**	**0.7522**	**0.7522**
6	22.7300	0.2171	0.7368	0.7867	0.7368
7	22.9736	0.2157	0.6842	0.8158	0.6842
8	23.2172	0.2145	0.6316	0.8416	0.6316
9	23.4608	0.2134	0.5789	0.8646	0.5789
10	23.7044	0.2124	0.5263	0.8853	0.5263
11	23.9481	0.2115	0.4737	0.9040	0.4737
12	24.1917	0.2107	0.4211	0.9210	0.4211
13	24.4353	0.2100	0.3684	0.9345	0.3684
14	24.6789	0.2094	0.3158	0.9473	0.3158
15	24.9225	0.2088	0.2632	0.9588	0.2632
16	25.1661	0.2083	0.2105	0.9694	0.2105
17	25.4097	0.2079	0.1579	0.9794	0.1579
18	25.6534	0.2074	0.1053	0.9886	0.1053
19	25.8970	0.2071	0.0526	0.9947	0.0526
20	26.1406	0.2069	0.0000	1.0000	0.0000

Table 5
Optimal values for here and now control variables at the best compromise solution (i.e. Solution#5) in Case-B.

Control variable	#	SMO-ORPD (Case-B)
Generator Control variable	V_{G1} (pu)	1.0445
	V_{G2} (pu)	1.0278
	V_{G3} (pu)	0.9991
	V_{G6} (pu)	0.9938
	V_{G8} (pu)	0.984
	V_{G9} (pu)	0.9799
	V_{G12} (pu)	1.009
Transformer Tap changer (pu)	T_1	1.0005
	T_2	0.9949
	T_3	0.9997
	T_4	0.9976
	T_5	0.9850
	T_6	0.9961
	T_7	0.9944
	T_8	1.0100
	T_9	0.9990
	T_{10}	0.9917
	T_{11}	0.9000
	T_{12}	1.0194
	T_{13}	0.9830
	T_{14}	0.9886

obtained. The proposed SMO-ORPD model is implemented on the IEEE 57-bus test system. The numerical results show that in the presence of wind power generation, the expected value of active power losses and L-index are decreased in comparison with the deterministic case. This implies the positive impact of wind power generation on the voltage stability enhancement and efficiency of the system.

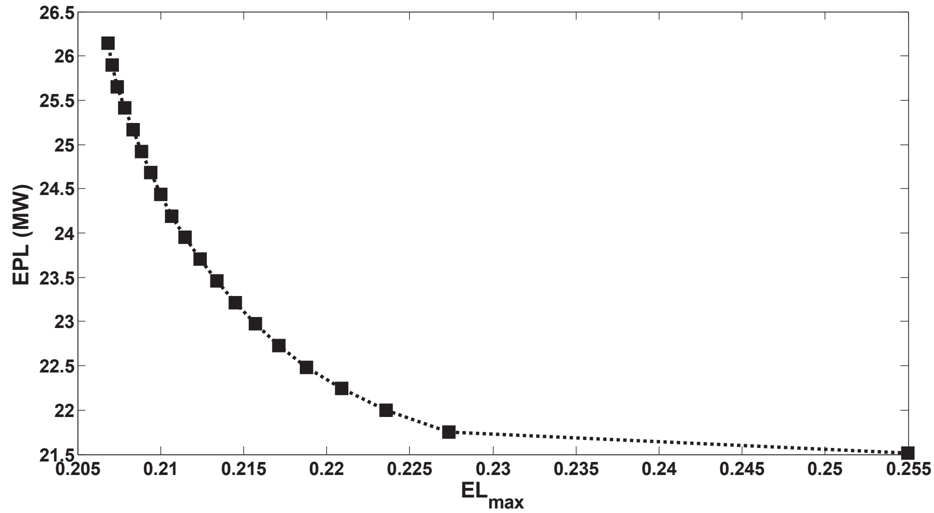

Fig. 7. Pareto front of SMO-ORPD (Case-B).

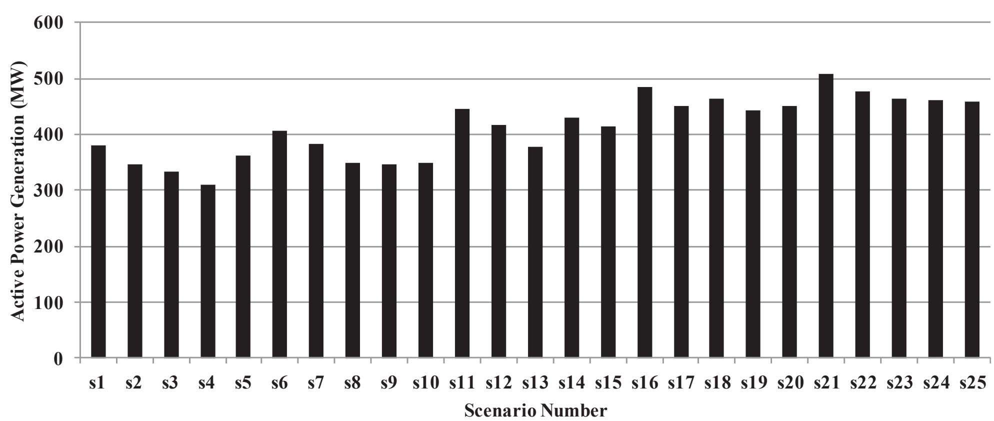

Fig. 8. Active power generation in slack bus (i.e. bus 1) in all scenarios (in MW).

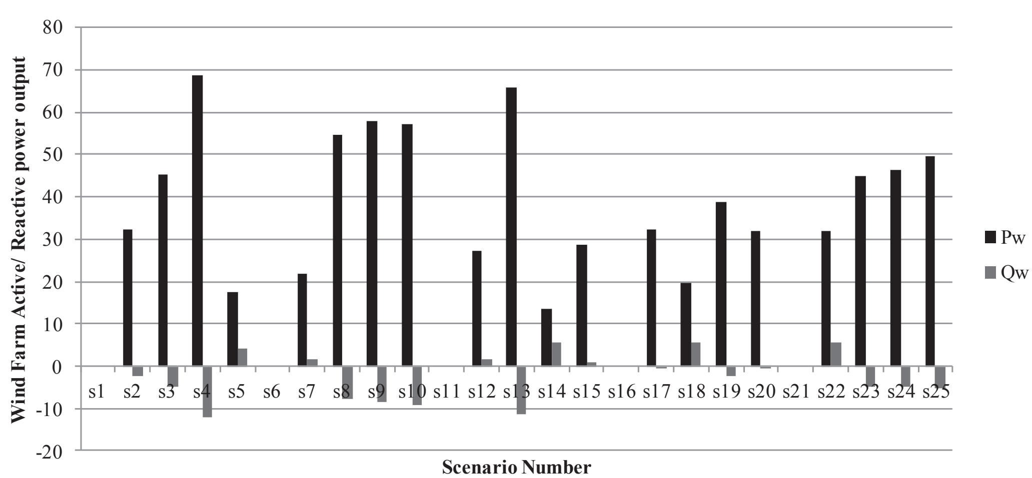

Fig. 9. Active and reactive power output of wind farm (located at bus 52) in all scenarios (in MW and MVAR).

At the future works, new uncertainty modeling techniques such as information gap decision theory (IGDT) and robust optimization (RO) will be utilized, since these approaches are powerful tools to deal with the problems in which no PDF or membership function is available regarding the uncertain parameters. Also, it is interesting to include the uncertainties associated with other forms of renewable energies such as photo-voltaic technology in the ORPD problem.

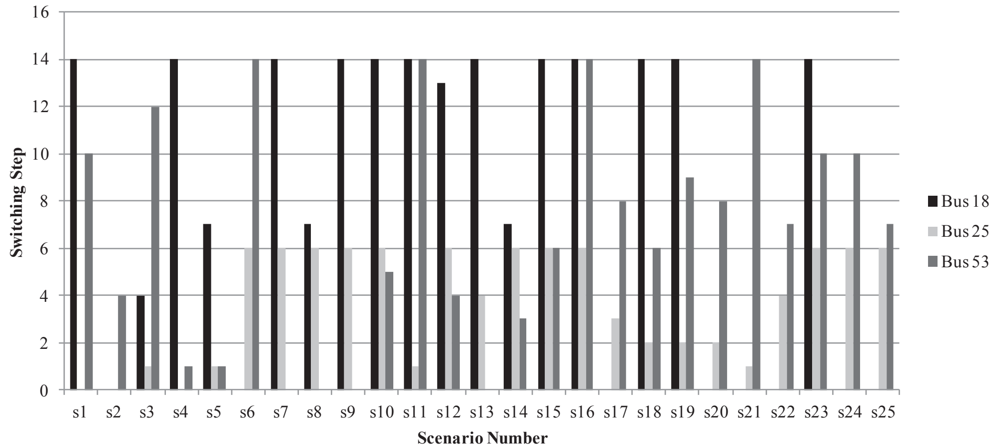

Fig. 10. Switching steps in VAR compensation buses 18, 25 and 53 at different scenarios.

Appendix

Table A1
The data of VAR Compensation devices

Bus no.	DMO-ORPD [47], [39]		SMO-ORPD		
	$Q_{C_i}^{min}$ (MVAR)	$Q_{C_i}^{max}$ (MVAR)	$I_{C_i}^{min}$	$I_{C_i}^{max}$	Q_{C_i} (MVAR)
18	0	10	0	14	0.5
25	0	5.9	0	6	0.5
53	0	6.3	0	14	0.5

References

[1] C. Dai, W. Chen, Y. Zhu, X. Zhang, Reactive power dispatch considering voltage stability with seeker optimization algorithm, Electr. Power Syst. Res. 79 (10) (2009) 1462–1471.
[2] A. Khazali, M. Kalantar, Optimal reactive power dispatch based on harmony search algorithm, Int. J. Electr. Power Energy Syst. 33 (3) (2011) 684–692.
[3] A. Ela, M. Abido, S. Spea, Differential evolution algorithm for optimal reactive power dispatch, Electr. Power Syst. Res. 81 (2) (2011) 458–464.
[4] R. Mallipeddi, S. Jeyadevi, P.N. Suganthan, S. Baskar, Efficient constraint handling for optimal reactive power dispatch problems, Swarm Evol. Comput. 5 (2012) 28–36.
[5] S. Duman, Y. Sönmez, U. Güvenç, N. Yörükeren, Optimal reactive power dispatch using a gravitational search algorithm, IET Gener. Transm. Distrib. 6 (2012) 563–576.
[6] D. Thukaram, G. Yesuratnam, Optimal reactive power dispatch in a large power system with AC-DC and FACTS controllers, IET Gener. Transm. Distrib. 2 (2008) 71–81.
[7] A. Rabiee, M. Parniani, Optimal reactive power dispatch using the concept of dynamic VAR source value, in: Power & Energy Society General Meeting, 2009 PES'09 IEEE, IEEE, 2009, pp. 1–5.
[8] M. Martinez-Rojas, A. Sumper, O. Gomis-Bellmunt, A. Sudrià-Andreu, Reactive power dispatch in wind farms using particle swarm optimization technique and feasible solutions search, Appl. Energy 88 (2011) 4678–4686.
[9] C.-M. Huang, S.-J. Chen, Y.-C. Huang, H.-T. Yang, Comparative study of evolutionary computation methods for active–reactive power dispatch, IET Gener. Transm. Distrib. 6 (2012) 636–645.
[10] A.Z. de Souza, R. Leme, K. Lo, J.S. de Souza, A. Almeida, Reactive power redispatch for loss reduction using a modified power flow Jacobian, IET Gener. Transm. Distrib. 6 (2012) 657–664.
[11] A. Rabiee, M. Vanouni, M. Parniani, Optimal reactive power dispatch for improving voltage stability margin using a local voltage stability index, Energy Convers. Manag. 59 (2012) 66–73.
[12] A. Khorsandi, A. Alimardani, B. Vahidi, S. Hosseinian, Hybrid shuffled frog leaping algorithm and Nelder–Mead simplex search for optimal reactive power dispatch, IET Gener. Transm. Distrib. 5 (2011) 249–256.
[13] M. Ghasemi, M.M. Ghanbarian, S. Ghavidel, S. Rahmani, E. Mahboubi Moghaddam, Modified teaching learning algorithm and double differential evolution algorithm for optimal reactive power dispatch problem: A comparative study, Inf. Sci. 278 (2014) 231–249.
[14] M. Ghasemi, S. Ghavidel, M.M. Ghanbarian, A. Habibi, A new hybrid algorithm for optimal reactive power dispatch problem with discrete and continuous control variables, Appl. Soft Comput. 22 (2014) 126–140.
[15] A. Rajan, T. Malakar, Optimal reactive power dispatch using hybrid Nelder–Mead simplex based firefly algorithm, Int. J. Electr. Power Energy Syst. 66 (2015) 9–24.
[16] E.M. Soler, E.N. Asada, G.R. Da Costa, Penalty-based nonlinear solver for optimal reactive power dispatch with discrete controls, IEEE Trans. Power Syst. 28 (2013) 2174–2182.
[17] Z. Hu, X. Wang, G. Taylor, Stochastic optimal reactive power dispatch: formulation and solution method, Int. J. Electr. Power Energy Syst. 32 (2010) 615–621.
[18] A. Rabiee, M. Parniani, Voltage security constrained multi-period optimal reactive power flow using benders and optimality condition decompositions, IEEE Trans. Power Syst. 28 (2013) 696–708.
[19] C.-F. Yang, G.G. Lai, C.-H. Lee, C.-T. Su, G.W. Chang, Optimal setting of reactive compensation devices with an improved voltage stability index for voltage stability enhancement, Int. J. Electr. Power Energy Syst. 37 (2012) 50–57.
[20] K. Khatua, N. Yadav, Voltage stability enhancement using VSC-OPF including wind farms based on genetic algorithm, Int. J. Electr. Power Energy Syst. 73 (2015) 560–567.
[21] N. Roy, H. Pota, M. Hossain, Reactive power management of distribution networks with wind generation for improving voltage stability, Renew. Energy 58 (2013) 85–94.
[22] L. Zhihuan, L. Yinhong, D. Xianzhong, Non-dominated sorting genetic algorithm-II for robust multi-objective optimal reactive power dispatch, Gener. Transm. Distrib. IET 4 (2010) 1000–1008.
[23] S. Jeyadevi, S. Baskar, C. Babulal, M. Willjuice Iruthayarajan, Solving multi-objective optimal reactive power dispatch using modified NSGA-II, Int. J. Electr. Power Energy Syst. 33 (2011) 219–228.
[24] A. Saraswat, A. Saini, Multi-objective optimal reactive power dispatch considering voltage stability in power systems using HFMOEA, Eng. Appl. Artif. Intell. 26 (2013) 390–404.
[25] B. Mandal, P.K. Roy, Optimal reactive power dispatch using quasi-oppositional teaching learning based optimization, Int. J. Electr. Power Energy Syst. 53 (2013) 123–134.
[26] B. Zhou, K. Chan, T. Yu, H. Wei, J. Tang, Strength Pareto Multi-group Search Optimizer for Multiobjective Optimal VAR Dispatch, 2014.
[27] G. Chen, L. Liu, P. Song, Y. Du, Chaotic improved PSO-based multi-objective optimization for minimization of power losses and L index in power systems, Energy Convers. Manag. 86 (2014) 548–560.
[28] A. Ghasemi, K. Valipour, A. Tohidi, Multi objective optimal reactive power dispatch using a new multi objective strategy, Int. J. Electr. Power Energy Syst. 57 (2014) 318–334.
[29] D. Santos-Martin, S. Arnaltes, J.R. Amenedo, Reactive power capability of doubly fed asynchronous generators, Electr. Power Syst. Res. 78 (2008) 1837–1840.
[30] M.E. Montilla-DJesus, D. Santos-Martin, S. Arnaltes, E.D. Castronuovo, Optimal operation of offshore wind farms with line-commutated HVDC link connection, Energy Convers. IEEE Trans. 25 (2010) 504–513.
[31] A. Rabiee, A. Soroudi, Stochastic multiperiod OPF model of power systems with HVDC-connected intermittent wind power generation, IEEE Trans. Power Deliv. 29 (1) (2014) 336–344.
[32] A. Brooke, D. Kendrick, A. Meeraus, GAMS Release 2.25: A User's Guide, GAMS Development Corporation, Washington, DC, 1996.
[33] P.E. Gill, W. Murray, M.A. Saunders, SNOPT: an SQP algorithm for large-scale

constrained optimization, SIAM J. Optim. 12 (2002) 979–1006.
[34] The GAMS Software Website (http://www.gams.com/dd/docs/solvers/sbb.pdf). 2013.
[35] A. Rabiee, A. Soroudi, B. Mohammadi-ivatloo, M. Parniani, Corrective voltage control scheme considering demand response and stochastic wind power, Power Syst. IEEE Trans. 29 (2014) 2965–2973.
[36] A. Soroudi, B. Mohammadi-Ivatloo, A. Rabiee, Energy Hub Management with Intermittent Wind Power. Large Scale Renewable Power Generation, Springer, Singapore, 2014, pp. 413–438.
[37] A. Soroudi, A. Rabiee, A. Keane, Stochastic real-time scheduling of wind-thermal generation units in an electric utility, IEEE Syst. J. (2014) (accepted for publication).
[38] M. Alipour, B. Mohammadi-Ivatloo, K. Zare, Stochastic risk-constrained short-term scheduling of industrial cogeneration systems in the presence of demand response programs, Appl. Energy 136 (2014) 393–404.
[39] C. Dai, W. Chen, Y. Zhu, X. Zhang, Seeker optimization algorithm for optimal reactive power dispatch, IEEE Trans. Power Syst. 24 (3) (2009) 1218–1231.
[40] C.A. Canizares, Voltage Stability Assessment: Concepts, Practices and Tools, Power System Stability Subcommittee Special Publication IEEE/PES, 2002. Final Document (thunderbox uwaterloo ca/~ claudio/claudio html# VSWG).
[41] H. Xiong, H. Cheng, H. Li, Optimal reactive power flow incorporating static voltage stability based on multi-objective adaptive immune algorithm, Energy Convers. Manag. 49 (5) (2008) 1175–1181.
[42] R. Raghunatha, R. Ramanujam, K. Parthasarathy, D. Thukaram, Optimal static voltage stability improvement using a numerically stable SLP algorithm, for real time applications, Int. J. Electr. Power Energy Syst. 21 (4) (1999) 289–297.
[43] X. Wang, Y. Gong, C. Jiang, Regional carbon emission management based on probabilistic power flow with correlated stochastic variables, IEEE Trans. Power Syst. 30 (2) (2014) 1094–1103.
[44] R.D. Christie, Power Systems Test Case Archive, Electrical Engineering Dept, University of Washington, 2000.
[45] R.D. Zimmerman, C.E. Murillo-Sánchez, D. Gan, A MATLAB Power System Simulation Package, 2005.
[46] S. Wen, H. Lan, Q. Fu, D. Yu, L. Zhang, Economic allocation for energy storage system considering wind power distribution, IEEE Trans. power Syst. 30 (2) (2015) 644–652.
[47] R.D. Zimmerman, C.E. Murillo-Sánchez, R.J. Thomas, MATPOWER: steady-state operations, planning, and analysis tools for power systems research and education, IEEE Trans. Power Syst. 26 (1) (2011) 12–19.